Journal of the Civil Engineering Forum, January 2026, 12(1):104-121
DOI 10.22146/jcef.22632
Available Online at https://jurnal.ugm.ac.id/v3/jcef/issue/archive

The Effect of Pyrolysis Temperature on the Performance of Sewage Sludge Biochar for Persulfate-based Oxidation of Bisphenol-A

Nurul Alvia Istiqomah[1*], Thi Vinh Nguyen[2], Dick Dick Maulana[2,3]
[1]Department of Civil and Environmental Engineering, Universitas Gadjah Mada, Yogyakarta, INDONESIA
[2]School of Civil, Environmental, and Architectural Engineering, Korea University, Seoul, Republic of KOREA
[3]Agrotechnology Program Study, Faculty of Agriculture, Universitas Islam Nusantara, Bandung, INDONESIA
*Corresponding author: nurulalviaistiqomah@ugm.ac.id

SUBMITTED 29 June 2025 **REVISED** 21 July 2025 **ACCEPTED** 15 September 2025

ABSTRACT Converting sewage sludge into biochar shows promise as an eco-friendly and cost-effective method for remediating pollutants. In this study, aerobic digested sewage sludge was evaluated as a low-cost carbon-based catalyst through a facile one-pot pyrolysis process. The sludge biochar (SBC) was then used as a persulfate (PS) activator for the degradation of Bisphenol-A (BPA). The effect of pyrolysis temperature on the physicochemical properties of SBC and catalytic activity was observed. Then, chemical quenching analysis was carried out to identify reactive species. Increasing the pyrolysis temperature from 350 to 700 °C resulted in an enhancement of the degradation rate constant of BPA from 0.95×10^{-2} min^{-1} to 8.9×10^{-2} min^{-1}. SBC pyrolyzed at 350 °C (A350), characterized by a high iron content (40%wt) in the form of amorphous Fe (e.g., ferrihydrite) and C=C functional group promoting the radical formation which is dominated by presence of hydroxyl radicals. However, iron in an amorphous form limited the catalytic activity of A350. By contrast, non-radical pathway dominates SBC pyrolyzed at 700 °C (A700) with highest BPA removal as the result of more hydrophobic nature (lower O/C) therefore attracting more BPA and PS to the biochar surface. Graphitic structure of A700 (lower I_D/I_G) supports the mediated electron transfer pathway for persulfate activation. A pH range of 2–9 and the of inorganic anions (e.g., Cl^-,NO_3^-,SO_4^-, and HCO_3^-) had negligible effects on the A700 system. This study introduces a novel approach to the value-added reuse of sewage sludge as an efficient persulfate activator for pollutant remediation with good resistance to water matrices conditions.

KEYWORDS Sewage sludge; Biochar; Persulfate activation; AOPs; BPA.

1 INTRODUCTION

Concern for the occurrence of organic micropollutants in water has been growing over the last decade, posing new challenges to the scientific community. Conventional water treatment methods have typically struggled to eliminate these micropollutants, whereas advanced treatments such as advanced oxidation processes (AOPs) have emerged as the most efficient solution (Kamal et al., 2024; Luo et al., 2014; Marleni et al., 2021). AOPs work by combining oxidants such as hydrogen peroxide and persulfate salts with activators which can be in the form of energy or catalysts. This combination generates free radicals capable of transforming pollutants into less harmful substances through mineralization (Yu, Feng, Tang, Pang, Zeng, Lu, Dong, Wang, Liu, Feng, Wang, Peng and Ye, 2020). Persulfate-based AOPs (PS-AOPs) with sulfate radicals as active species are superior due to their higher redox potential, longer half-life, and wider operative pH compared to traditional hydroxyl radical-based AOPs (Hu, Wang, Shen, Wang, Wang, Xu, Zheng and Zhang, 2020). Furthermore, PS-AOPs are less expensive to store and transport because of the abundant availability of persulfate salts (Lee et al., 2020).

Carbonaceous materials have gained increasing recognition as an alternative to metals and metal oxides in the field of PS-AOPs catalysis due to their lower risk of metal leaching and comparable efficiency (Zhou et al., 2021). Biochar stands out as a highly effective catalyst among carbonaceous materials because of its efficiency and availability (Gasim et al., 2022). Its surface functional groups and structural defects effectively donate electrons to break the peroxide bond in persulfate, generating reactive radicals that enhance the oxidation process (Li et al., 2020). In addition, its large specific surface area, porous structure, abundant functional groups, and mineral-rich composition promote effective interactions with both persulfate and target pollutants (Lee et al., 2020). Moreover, a life cycle assessment study revealed that the cumulative energy demand of biochar production is approximately 80% less than that of activated carbon (Shaheen et al., 2022). Consequently, the use of biochar for persulfate activation continues to be explored, with researchers investigating various feedstock sources (Song et al., 2022).

As sewage sludge is a waste material that requires treatment, the conversion of sewage sludge into biochar for pollutant remediation presents an environmentally friendly and cost-effective solution that has garnered significant interest for further research (Mian et al., 2019; Wang, Liao, Ifthikar, Shi, Du, Zhu, Xi, Chen and Chen, 2017). The processing of sewage sludge typically represents a substantial portion (40%–60%) of the total operational costs in wastewater treatment plants (Guo et al., 2013). Given the high energy consumption associated with sewage treatment facilities, the conversion of sewage sludge into biochar could contribute to efforts aimed at reducing sludge accumulation (Ji et al., 2022). Aerobic and anaerobic digestion are two common processes used in sewage treatment for the decomposition of organic matter. In contrast to anaerobic sludge, aerobically digested sludge tends to undergo a higher degree of humification, potentially leading to lower levels of dissolved organic matter (Shao et al., 2013). This decrease in dissolved organic matter is reported to be beneficial for the production of biochar with a large surface area and an increased degree of graphitization, which facilitates electron transfer. Furthermore, the dissolved organic matter in sludge has been identified as having a toxic effect on the biochar produced (Zhou et al., 2023). Despite its beneficial potential properties, aerobic sludge has often been overlooked and warrants further research.

In biochar production, aside from the composition of the sludge source, pyrolysis parameters also play a vital role in shaping the physicochemical properties of biochar and therefore its performance and mechanism in pollutant removal via PS-AOPs (Zielińska et al., 2015). Different temperature conditions during pyrolysis induce physicochemical transformations in biomass, which leads to changes in the properties of the resulting biochar. It has been observed that nitrogen and carbon elements become enriched with heterocyclic aromatic structures in the biochar as the pyrolysis temperature rises. Additionally, as the temperature increases up to 700 °C, thermal transformation from an amorphous phase to a graphitic crystalline structure occurs in a disordered manner (Keiluweit et al., 2010). These properties of biochar determine its interaction with persulfate and pollutants, thereby influencing its oxidation performance and mechanism (Ghodake et al., 2021).

Although the effect of biochar pyrolysis temperature on the pollutant removal efficiency of PS-AOPs has been widely discussed (Chen, Duan, Zhang, Wang, Ren and Ho, 2020; Pei et al., 2021; Wang, Gu, Zhou, Zhu, Li, Tao, Wen and Zhang, 2017), there remains a lack of understanding about the use of biochar derived from aerobic sewage sludge in PS-AOPs for Bisphenol A (BPA) degradation. BPA is used as a model contaminant because of its widespread prevalence and toxicity. It is used extensively in the plastic industry as a key monomer for various chemical materials, including polycarbonate plastic resin, epoxy resin, and polycarbonate. The detection of BPA in surface water has steadily risen worldwide over the past two decades (Corrales et al., 2015). Studies on the toxic effects of BPA have revealed that even very low concentrations can cause respiratory irritation and exhibit estrogenic activity (Ginter-Kramarczyk et al., 2022). Consequently, BPA has been recognized as a representative endocrine-disrupting chemical by the US Environmental Protection Agency (Diao et al., 2020).

Therefore, in this study, aerobic sewage sludge was converted into biochar and used as a low-cost, carbon-based catalyst for PS-AOP in BPA degradation. Peroxydisulfate (PDS) was chosen as the precursor for persulfate because of its higher standard redox potential and lower dissociation energy compared to peroxymonosulfate (PMS). Various techniques were employed to characterize the intrinsic physicochemical properties of sludge biochar (SBC). The impact of pyrolysis temperature on the physicochemical properties of SBC and its catalytic activity in BPA degradation kinetics were observed. The generation of reactive oxidizing species was confirmed through radical quenching experiments using carefully selected chemicals. Additionally, mechanisms that underlie persulfate activation and pollutant degradation were proposed. Furthermore, the influence of different water matrices, including pH and inorganic anions, was investigated to assess the potential applicability of the system.

2 MATERIALS AND METHODS

2.1 Chemicals and reagents

All chemicals used in the experiments were analytical reagent grade. Bisphenol A ($C_{15}H_{16}O_2$, ⩾ 99%) and sodium persulfate ($Na_2S_2O_8$, 99%) were purchased from Sigma Aldrich Inc., USA. Potassium iodide (KI, 99%) and sodium bicarbonate ($NaHCO_3$, 99.7%) for the PS decomposition test were purchased from J.T. Baker, USA. Quenching chemicals including tert-Butyl alcohol, methanol, p-benzoquinone, chloroform, and L-histidine and inorganic anions including potassium nitrate, potassium bicarbonate, potassium chloride, and potassium sulfate were purchased from Daejung Chemical Co., Korea. The solution pH was adjusted using 0.1 M sodium hydroxide (NaOH) and 0.1 M sulfuric acid (H_2SO_4) (Duksan Pure Chemicals, Korea). The deionized water (DIW) used in these experiments for the preparation of the reagents was purified via the Millipore reverse osmosis purification system.

Table 1. Chemical used as scavengers for active species quenching this study

No	Chemical	Log Pow	Target	$k_2(M^{-1}s^{-1})$	Ref
1	Methyl alcohol	-0.77	•OH	9.7×10^8	Wu et al. (2021)
			$SO_4^{\bullet-}$	2.5×10^7	
2	tert-Butyl alcohol	0.35	•OH	$(3.8\text{-}7.6) \times 10^8$	
			$SO_4^{\bullet-}$	$(4\text{-}9.1) \times 10^5$	
3	p-Benzoquinone	0.20	$O_2^{\bullet-}$	$(0.9\text{-}1) \times 10^9$	Hu, Tong, Li, Xie, Chen, Wen, Feng, Wang, Li, Wang and Zhang (2020)
			•OH	6.6×10^9	Chen et al. (2018); Li et al. (2019); Oh et al. (2017)
			$SO_4^{\bullet-}$	1×10^8	
4	Chloroform	1.97	$O_2^{\bullet-}$	3×10^{10}	Hwang et al. (2010)
			•OH	5×10^6	
			$SO_4^{\bullet-}$	$\sim 10^7$	Tratnyek et al. (2009)
5	L-histidine	-	$^1O_2$	3.2×10^7	Wilkinson et al. (1995*a*)

2.2 Preparation of sludge biochar

The sewage sludge was obtained from a secondary sedimentation tank at the Jungnang Sewage Treatment Plant in Seoul, South Korea. This tank received sludge from the plant's activated sludge treatment unit. After collection, the sludge was dried at 105 °C for 24 hours in a drying oven. A specific quantity of the dried sludge was then placed into a quartz tube and subjected to pyrolysis in a tube furnace. The pyrolysis process to the target temperature lasted for 2 hours by increasing the temperature at a rate of 5 °C min^{-1} with 100 mL min^{-1} of N_2 sweeping as inert shielding gas. The N_2 atmosphere was maintained until the pyrolysis process ended and the temperature in the furnace decreased to room temperature.

The temperatures of 350 °C, 500 °C, and 700 °C were chosen as the target temperatures. A temperature of 350 °C was selected because at temperatures below 500 °C, the presence of nitrogen content is expected to be higher, resulting in the production of more free radicals (Wu et al., 2021). However, at less than 350 °C, aliphatic carbon dominates with a lower presence of aromatic carbon. In other words, the structure of the biomass does not change significantly because of incomplete carbonization (Chen, Wang, Duan, Wang, Ren and Ho, 2020; Leng et al., 2021). Starting at 400–500 °C, as the temperature increases, amorphous carbons transform into crystalline carbons via condensation. More volatiles are removed, creating sparse regions, which leads to cracks in the material and generates more pores (Leng et al., 2021). A higher temperature of 700 °C is considered a highly graphitic temperature (Wu et al., 2021) at which biochar loses its surface functionality because of more aromatic condensation reactions. However, at a temperature of 750 °C, a nearly complete loss of biochar surface functional groups can occur (Janu et al., 2021). The resulting SBC from the pyrolysis process was ground and passed through a 30-mesh sieve (600 µm) without further activation. The sludge biochar was denoted as A350, A500, and A700for pyrolysis temperatures of 350 °C, 500 °C, and 700 °C, respectively.

2.3 Characterization of biochar

The elemental (C, H, N, O, S) analysis of the SBC was conducted using the vario MICRO cube (Elementar, Germany). The elemental (Mn, Fe, Cu, Zn) analysis of the SBC was carried out using energy dispersive X-ray fluorescence spectroscopy (Hitachi SEA1200VX). Fourier transform infrared (FT-IR) spectroscopic analysis was performed to probe the surface structures of SBC using a Cary 630 FT-IR (Agilent). Raman spectra (LabRam ARAMIS IR2, Horiba Scientific, France) were employed to explore the defective and graphitic structures of SBC. An X-ray diffractometer (SmartLab, Rigaku, Japan) was used to analyze the crystalline structures in SBC. The zeta potentials were measured by the Zeta Potential Analyzer (ELSZ-1000, Otsuka Electronics, Japan). A nitrogen adsorption–desorption apparatus was employed to determine the Brunauer–Emmett–Teller specific surface area and Barret–Joyner–Halenda pore size distribution at 77 K and degassing at 393 K.

2.4 Batch experiment

The BPA degradation experiments were conducted in a 500 mL glass beaker with 100 mL of reaction solution at room temperature. The catalyst dosage was 1 gL^{-1}, the PDS concentration was 1 mM, the initial pH was the natural pH of the BPA solution (approximately 5.8), and the BPA concentration was 0.2 mM (50 mgL^{-1}). All the reactions were stirred constantly to disperse the SBC in the solution. First, the sludge biochar was added to the solution and was stirred for 60 minutes to achieve adsorption equilibrium. The adsorption equilibrium test is shown in Figure S1. The activation process of BPA degradation was started by adding a cer-

Table 2. Physicochemical characteristics of SBC

Sample	Yield (%)	S_{BET} (m^2g^{-1})	Pore vol.	Organic element (wt%)							Inorganic element (wt%)				pH_{pzcc}
				C	H	N	S	O	O/C	H/C	Mn	Fe	Cu	Zn	
A-350	65.2	51.4	0.18	23.2	2.4	2.0	0.5	18.9	0.84	0.11	1.25	40.01	0.74	1.34	2.25
A-500	58.0	61.5	0.19	20.9	1.7	5.0	0.19	17.7	0.82	0.08	2.45	32.22	0.75	1.67	3.2
A-700	47.2	46.0	0.18	21.2	0.9	4.4	0.11	11	0.52	0.05	2.28	31.43	0.76	1.60	2.6

tain amount of PDS to the BPA solution with sludge biochar. At each time interval, 1 mL of solution was filtered through a 0.22 µm Millipore film and mixed with 1 mL of methanol to completely terminate the oxidation.

To investigate the pH effect, a range of pH values, 3.0, 5.0, 7.0 and 9.0, was applied using 0.1 M NaOH and H_2SO_4, and the experiment was explored without buffer control (during the experiments, no steps were taken to adjust the value of the pH). Moreover, to observe the effect of coexisting inorganic ions, anions with a concentration of 10 mM (i.e., Cl^-, NO_3^-, SO_4^{2-}, and HCO_3^-) were added to the system. The rate of PDS consumption was detected by using a previously reported spectrophotometric method (Gokulakrishnan et al., 2016; Liang et al., 2008).

2.5 Quenching experiment of reactive oxygen species

Quenching experiments are applied to investigate the main reactive oxygen species (ROS), which contributes to pollutant degradation using high kinetic scavengers (Zhang et al., 2018). The compilation of the scavenging compound used in this study is shown in Table 1. With the initial assumption that there are four possible ROS produced that potentially react with the pollutants, hydroxyl radical (•OH), sulfate radical ($SO_4^{\bullet-}$), superoxide radical ($O_2^{\bullet-}$), and singlet oxygen ($^1O_2$). tert-Butyl alcohol (TBA) is used to quench •OH, while methyl alcohol (MeOH) is applied to quench both •OH and $SO_4^{\bullet-}$ (Wu et al., 2021). p-Benzoquinone (pBQ) is used to equally scavenge •OH,$SO_4^{\bullet-}$,$O_2^{\bullet-}$ (Hu, Tong, Li, Xie, Chen, Wen, Feng, Wang, Li, Wang and Zhang, 2020). Moreover, chloroform has been reported specifically to have high kinetic constant for $O_2^{\bullet-}$ (Hwang et al., 2010). Using a combination of TBA and chloroform would enable the quenching of •OH,$O_2^{\bullet-}$. In addition, the presence of $^1O_2$ is quenched using L histidine (Wilkinson et al., 1995*b*). Referring to the Log Pow value in Table 1, and considering the relatively low solubility of MeOH, TBA, pBQ, and L-histidine, these compounds were used at a PDS/scavenger concentration of 1:500. In contrast, chloroform, which has higher solubility in water than the others, was used at a PDS/scavenger concentration of 1:10.

3 RESULTS AND DISCUSSION

3.1 Properties of sludge biochar

The physicochemical properties of SBC are detailed in Table 2. One notable trend observed is the reduced yield of the biochar with increasing temperatures. This decline is likely associated with the loss of chemically bound H_2O content, organic matter degradation, and the release of CO and CO_2, coupled with the development of an aromatic structure (Gopinath et al., 2021; Zielińska et al., 2015). The surface area peaked at 500 °C, accompanied by a larger pore volume than other kinds of SBCs. The decrease in surface area with increasing temperature up to 700 °C may be attributed to a higher ash content. The adverse effect of ash on the surface area might result from pore filling or blockage by inorganic compounds (Zielińska et al., 2015). The melting of ash content above 500 °C fills the pores, consequently reducing the surface area (Ronsse et al., 2013).

As the pyrolysis temperature increases, a decrease in the H/C and O/C ratios is observed compared to the initial concentrations in the raw sludge (see Table S1 Appendix A). A lower H/C ratio indicates enhanced carbonization, which indicates abundant unsaturated structures due to substantial degasification (Zielińska et al., 2015). With a rising temperature, the decline in the O/C ratio results from dehydration reactions, leading to a less hydrophilic biochar surface. Consequently, biochar becomes more hydrophobic because of significant oxygen removal. Furthermore, the decrease in oxygen content at elevated temperatures is attributed to the elimination of acidic functional groups, resulting in a more alkaline biochar surface.

As pyrolysis temperature increases, most inorganic elements—excluding iron (Fe)—tend to accumulate or remain stable due to their low volatility, resulting in higher concentrations at elevated temperature (Pariyar et al., 2020). Zinc (Zn) is not redox-active under typical conditions and thus does not significantly activate persulfate. While Copper (Cu) can generate sulfate radicals via electron donation, its consistent concentration across samples (0.75 ± 0.01 wt%) limits further discussion. Manganese (e.g., Mn^{2+}/Mn^{2+}) may activate persulfate via redox cycling, but the process is slower and

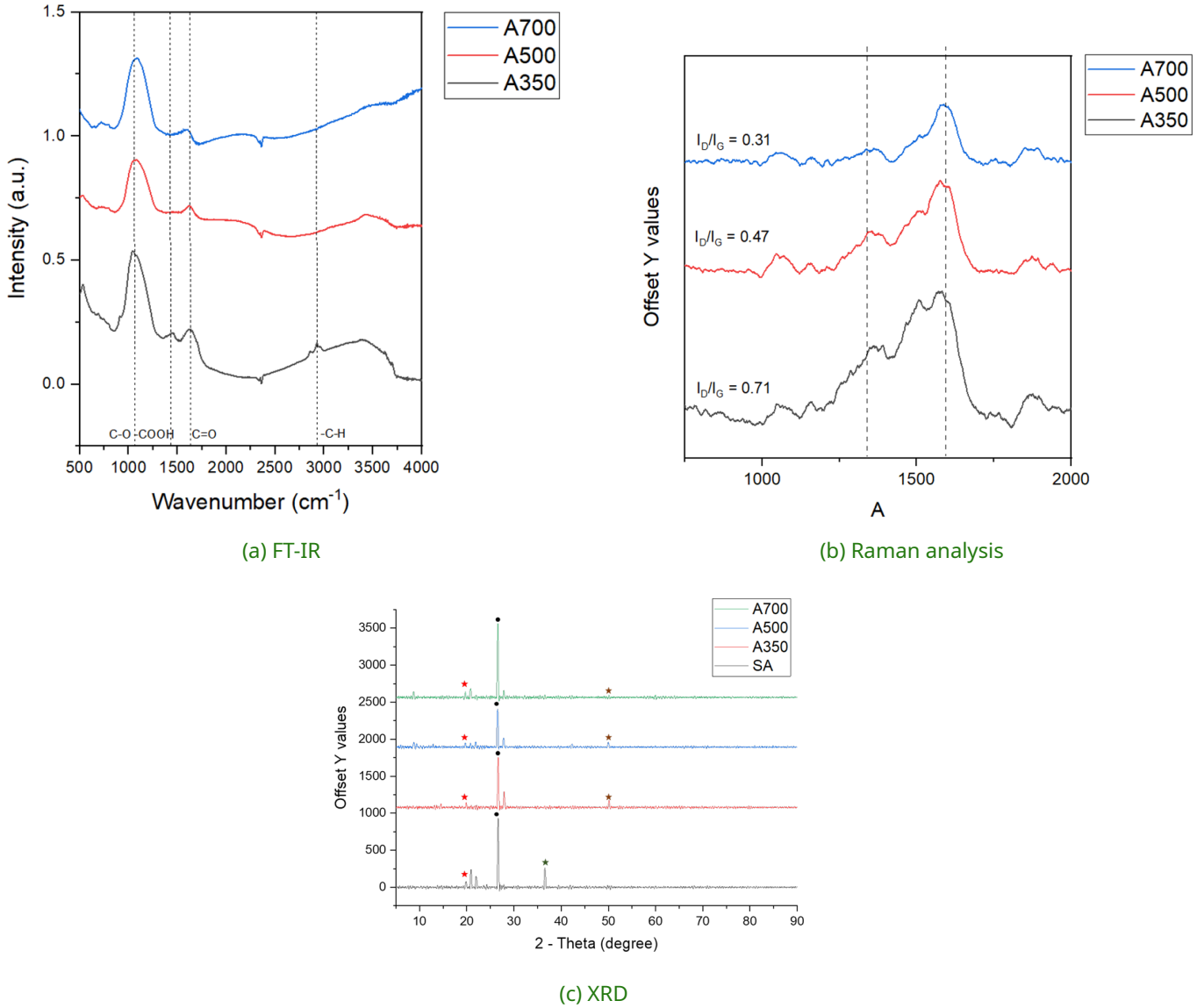

(a) FT-IR

(b) Raman analysis

(c) XRD

Figure 1 Characterization of SBC by: (a) FT-IR, (b) Raman analysis, and (c) XRD.

less efficient (Zhou et al., 2024). Therefore, these metals are not discussed further as possible active sites.

The amount of Fe content decreases from A350 to A700, possibly because of volatilization and chemical reactions as the pyrolysis temperature rises. The thermochemical reduction of iron oxide is also observed with increasing pyrolysis temperatures in other types of sludge-derived biochar (Wang, Gu, Zhou, Zhu, Li, Tao, Wen and Zhang, 2017). The points of zero charge (pH_{pzc}) for all types of SBC fall within the range of 2.2–3.2, which would influence subsequent adsorption and catalytic processes (Pariyar et al., 2020).

The FT-IR results in Figure 1a reveal the presence of oxygen functional groups in the SBC. Notably, A350 exhibits a broader peak spectrum, suggesting a greater availability of surface functional groups. The notably elevated carbonyl (C=O) levels in A350 may indicate the presence of ketones in this type of biochar (Ronsse et al., 2013). In addition to the heightened C=O stretching peak, A350 displays peaks associated with hydrocarbons (C-H) stretching and carboxyl (-COOH) compared to A500 and A700, indicating limited structural alterations in the biomass due to incomplete carbonization (Pariyar et al., 2020).

The Raman spectra presented in Figure 1b indicate specific adsorption peaks at 1330 cm^{-1} (D-band) and 1560 cm^{-1} (G-band) in all SBC samples, where the intensity ratio I_D/I_G reflects the degree of graphitization of carbons (Xiao et al., 2022). A higher I_D/I_G ratio indicates a higher presence of defective sites that can serve as electron donors, whereas a lower I_D/I_G value signifies a more graphitized structure, which is beneficial for electron transfer mechanisms (Chen, Wang, Duan, Wang, Ren and Ho, 2020). Analysis of the Raman data reveals that the value of the I_D/I_G ratio decreases with increasing pyrolysis temperature, reaching its lowest point at 700 °C.

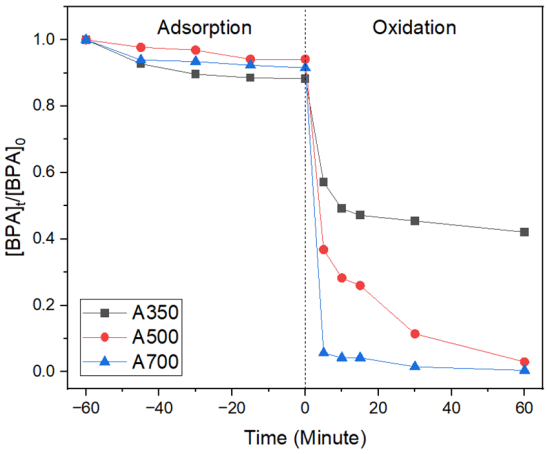

(a) Adsorption and oxidation process

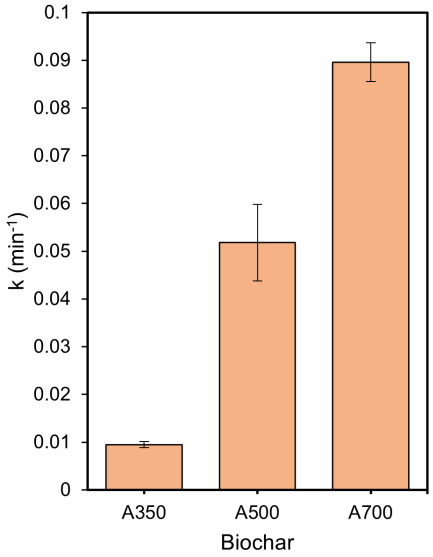

(b) Kinetic rate constant value

Figure 2 Degradation kinetics of BPA expressed in (a) adsorption and oxidation process, (b) kinetic rate constant value. (Biochar = 1g L^{-1}; $[BPA]_0$ = 50mg L^{-1}; $[PDS]_0$ = 1 mM; and T = 298 K, initial pH = 5.8 ± 0.1).

The XRD results in Figure 1c indicate the presence of iron in the form of Fe_3O_4 (JCPDS No. 19-0629) (Shao et al., 2022). Furthermore, all kinds of SBC exhibit a peak at 26.5, attributed to SiO_2 (JCPDS card No. 89-8936), which originates from the sewage sludge precursor (Hu, Tong, Li, Xie, Chen, Wen, Feng, Wang, Li, Wang and Zhang, 2020). It has been reported that the silicon in sludge-derived biochar cannot be neglected because of the large amount of grit and sand carried in sludge (Song et al., 2022). A700 shows the highest silica content, which promotes the decrease of the surface area due to pore clogging (Hu, Tong, Li, Xie, Chen, Wen, Feng, Wang, Li, Wang and Zhang, 2020).

3.2 Catalytic performance

As biochar also functions as an adsorbent, the kinetics of BPA adsorption were examined using the pseudo-first-order and pseudo-second-order kinetic models as described in Text S1. The kinetic parameters for the adsorption of BPA by sludge biochar are presented in Table S2 Appendix A. Comparing the two kinetic models, the correlation coefficient values (R2) for the pseudo-second order model are higher for all types of SBC (R2 = 0.90 – 0.98). This suggests that the pseudo-second-order model accurately describes the adsorption process, indicating a chemisorption mechanism in which the surface reaction is the rate-limiting step (Zhou et al., 2023). Although all kinds of SBC show similar times to reach apparent equilibrium (within 60 minutes, as shown in Figure S1, their adsorption capacities are relatively low. Notably, A500 exhibits the highest adsorption capacity, likely because of its larger surface area. The low adsorption capacity of A350 might be attributed to its low surface area, which is caused by the pore-blocking effects of dissolved organic matter (DOM) as this type of biochar shows a higher yield than others. A higher yield leads to a significant portion of uncarbonized or partially carbonized material in the biochar, which is the source of DOM. While the presence of DOM is outside the scope of this study, it has been reported that DOM in biochar prepared at lower pyrolysis temperatures suppresses adsorption capacity and further hinders its catalytic performance (Zhou et al., 2023).

BPA is an organic compound with hydrophilic hydroxyl groups and hydrophobic aromatic groups (Zhou et al., 2014). Consequently, the adsorption mechanism can be attributed to hydrophobic bonding between the benzene ring of biochar and the C=C of BPA (Mpatani et al., 2021), particularly considering the low O/C ratio (indicating higher aromaticity and hydrophobicity) of A500 and A700. Additionally, BPA is a weakly acidic compound that ionizes at specific pH levels. The pH_{pzc} for sludge biochar averages between 2 and 3 (Table 2). Adsorption occurs at a non-adjusted pH of 5.8, where pH > pH_{pzc} indicates a negatively charged surface and pH < pKa of BPA (9.6) implies that BPA remains in its non-dissociated form. Consequently, the low adsorption capacity of sludge biochar can be attributed to weak dispersive interactions which result from unfavorable pH conditions (Fan et al., 2021).

To focus solely on the oxidation process, persulfate was added after reaching adsorption equilibrium (60 minutes). As depicted in Figure 2a, adsorption alone accounts for less than 20% of BPA removal, and the degradation of BPA is hastened with the addition of PDS. The efficient degradation of BPA was observed in A700 with a rate constant of $8.96 \times 10^{-2} min^{-1}$ and a nearly complete removal within 30 minutes. A500 and A350 exhibit slower degradation rates, with rate con-

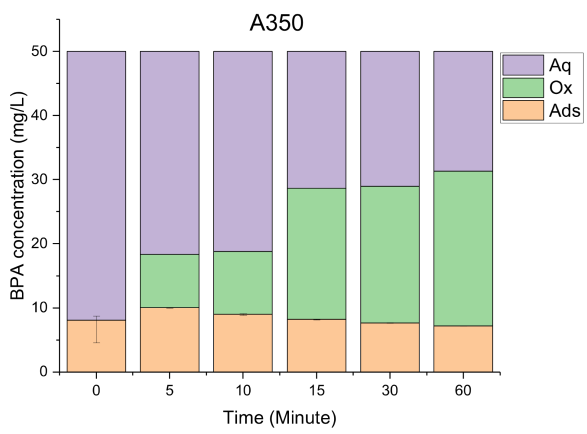

(a) A700

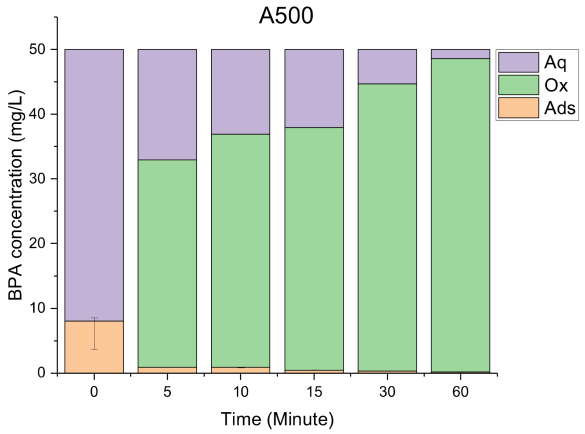

(b) A500

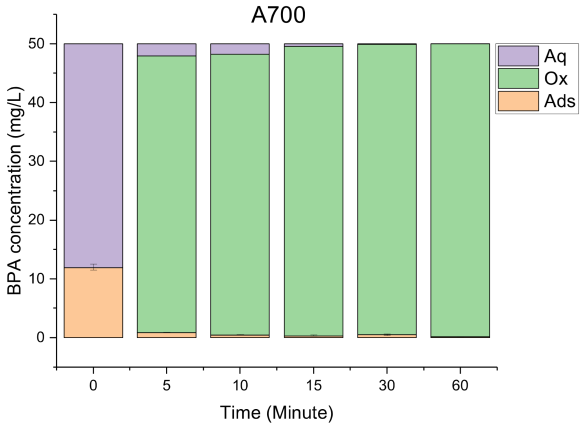

(c) A350

Figure 3 Concentration fractions of adsorbed, oxidized, and remaining BPA in the PS-AOP system using biochar: (a) A700, (b) A500, and (c) A350. Experimental conditions: Biochar = 1g L^{-1}; $[BPA]_0$ = 50mg L^{-1}; $[PDS]_0$ = 1 mM; and T = 298 K, initial pH = 5.8 ± 0.1

stants of 5.18 × $10^{-2}$$min^{-1}$ and 0.95 × $10^{-2}$$min^{-1}$, respectively (Figure 2b). The enhanced hydrophobicity and graphitic structure of A700 likely contribute to the accelerated degradation of BPA. Compared with similar catalytic systems that use carbonaceous materials for BPA degradation, the proposed SBC/PS system possesses superior catalytic performance in terms of the reaction rate constant despite its simple preparation method (Table S3 Appendix A).

To distinguish the individual contributions of adsorption and oxidation, the removed BPA is segmented into three primary fractions: adsorbed BPA, oxidized BPA, and dissolved BPA remaining in the solution. This procedure involves collecting biochar samples at specific intervals during the batch test. The BPA content within the biochar is then determined by dissolving the biochar in methanol, and the resulting supernatant is analyzed using High-Performance Liquid Chromatography (Zhou et al., 2015). The detected BPA concentration represents the adsorbed BPA within the biochar. The fraction of oxidized BPA is calculated by comparing the remaining BPA in both its adsorbed and dissolved forms with the initially added pollutants, as expressed in Equation (1):

$$f_{deg(x)} = 1 - (f_{ad(pre)} + f_{ad(x)}) - f_{aq} \quad (1)$$

where $f_{ad(pre)}$ and $f_{ad(x)}$ represent the fraction of adsorbed BPA before the addition of PDS and during the specified time (x indicates the time, measured from the solid by acid desorption), respectively. f_{aq} is the fraction of freely dissolved BPA in the solution, and f_{deg} is the fraction of oxidatively degraded BPA. All fraction values are expressed in mg L^{-1}.

At the initial stage (minute 0), before the addition of PDS, adsorption stands out as the sole removal mech-

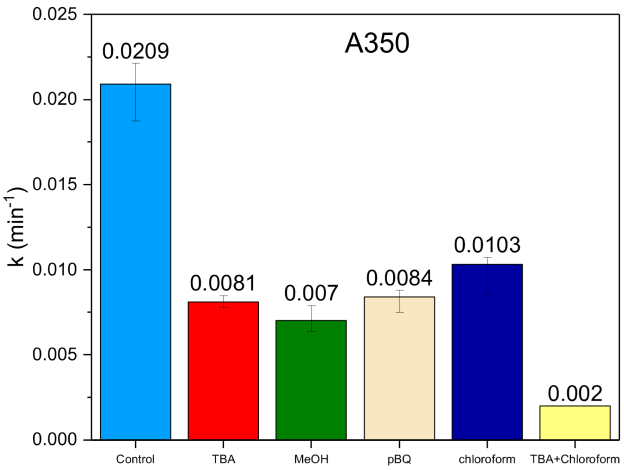

(a) A350

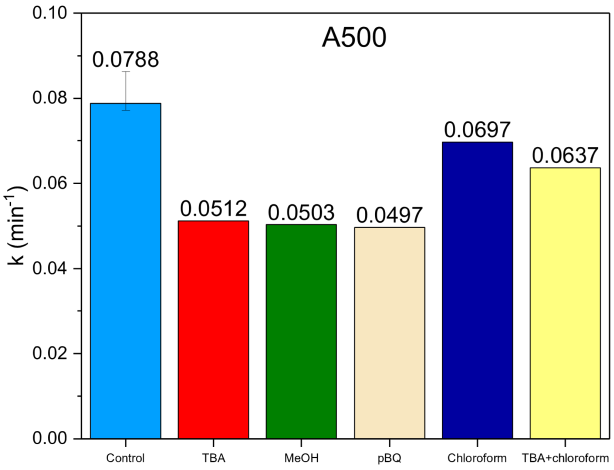

(b) A500

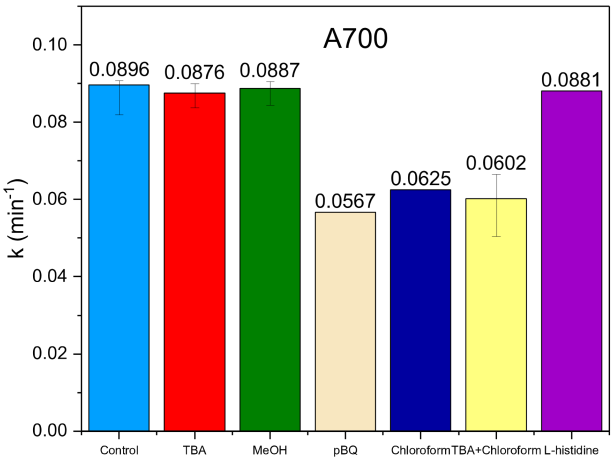

(c) A700

Figure 4 Quenching effect on BPA degradation rate constant by PS-AOP activated biochar: (a) A350, (b) A500, and (c) A700. Experimental conditions: Biochar = 1g L^{-1}; $[BPA]_0$ = 50mg L^{-1}; $[PDS]_0$ = 1 mM; and T = 298 K, initial pH = 5.8 ± 0.1; TBA, MeOH, pBQ, and L-histidine to PDS ratio= 500:1; chloroform to PDS ratio= 10:1

anism observed in all systems, as illustrated in Figure 3. Following the addition of PDS, oxidation becomes the dominant process, with less than 2% additional adsorption occurring thereafter in A700 and A500 (Figure 3a and 3b). However, further adsorption was still observed in A350 with a lower fraction of oxidated BPA than A700 and A500 (Figure 3c). Overall, the removal of BPA in A700 and A500 is driven mainly by the oxidation process, which indicates that these two types of SBC are suitable as catalysts for persulfate activation. In the A350 system, both adsorption and oxidation contribute to the removal mechanism.

3.3 Mechanism study

Quenching experiments were conducted to investigate the contributions of radical pathways and identify the reactive species involved. This method relies on variations in reactivity and reaction rates between reactive species and specific chemical scavengers. Both the selectivity of the scavenger toward the target reactive species and the ratio of scavenger concentration to oxidant are crucial considerations in the quenching test (Wang et al., 2020).

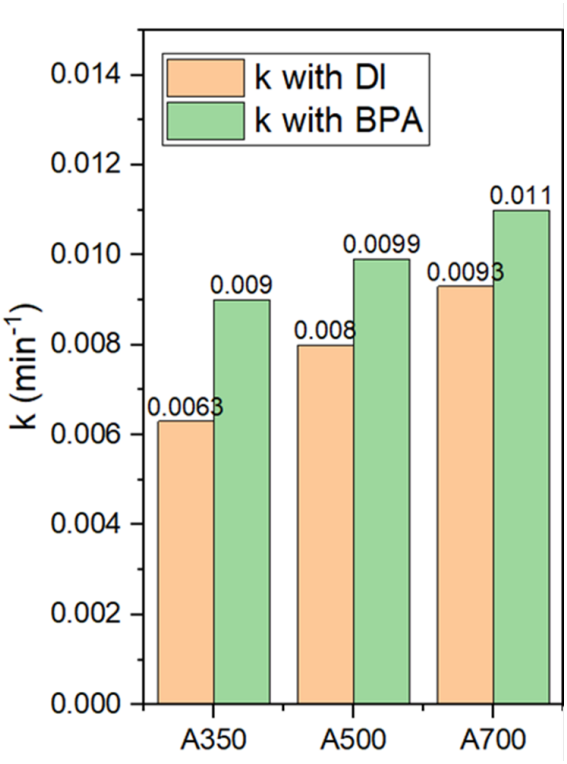

Figure 5 PDS consumption rate with and without the presence of BPA (*p*-values of all samples < 0.05). Experimental conditions: Biochar = 1 g L^{-1}; $[BPA]_0$ = 50 mg L^{-1} when present, or 0 mg L^{-1} when absent; $[PDS]_0$ = 1 mM; and T = 298 K, initial pH = 5.8 ± 0.1

As depicted in Figure 4, different scavengers exhibited varying degrees of inhibition in the rate constant of BPA degradation. In the A350 system, all scavengers caused a greater than 50% decrease in the rate constant (Figure 4a). Since most of the scavengers used have comparatively high reactivity toward •OH (Table 1), it can be inferred that •OH is the predominant active species in the A350 system. Moreover, considering that •OH can be generated from the primary product $SO_4^{\bullet-}$ by reacting with H_2O (Wu et al., 2021).

As depicted in the A500 system in Figure 4b, the effect of scavengers is less pronounced than in A350, which indicates some nonradical involvement, along with a combination of •OH, $SO_4^{\bullet-}$, $O_2^{\bullet-}$. The impact of all scavengers except for pBQ and chloroform is reduced in the A700 system, which suggests strong involvement of $O_2^{\bullet-}$ in BPA degradation with some contribution from nonradical pathways (Figure 4c). The dominance of $O_2^{\bullet-}$ could also be attributed to the decomposition of PDS following Equation (2) and (3) (Wang et al., 2020; Zhao et al., 2020).

$$S_2O_8^{2-} + 2H_2O \rightarrow HO_2^- + 3H^+ + SO_4^{2-} \quad (2)$$

$$S_2O_8^{2-} + HO_2^- \rightarrow SO_4^{\bullet-} + H^+ + O_2^{\bullet-} + SO_4^{2-} \quad (3)$$

Additionally, L-histidine is used to probe the effect of $^1O_2$; however, no significant decrease in the rate constant is observed. The effect of $^1O_2$ may be negligible in this system because of the low reactivity of BPA and $^1O_2$ ($k_2 = 3 \times 10^5 M^{-1}s^{-1}$) (Chu et al., 2019).

To further investigate the contribution of nonradical pathways, the rate of PDS consumption was analyzed with and without the presence of BPA in the system during the reaction. It was assumed that the nonradical pathway occurs through direct electron transfer from BPA (electron donor) to PDS (electron acceptor) mediated by biochar. Figure 5 shows a significant increase in the PDS consumption rate upon the addition of BPA as an electron donor. This is supported by the *t*-test result, where the *p*-value is less than 0.05, which suggests a significant difference between the two groups (shown in Table S4 Appendix A). In this case, the presence of biochar plays a crucial role in ensuring the mass transport and adsorption of both BPA and PDS, which is critical for efficient electron transfer from BPA to PDS (Cheng et al., 2017; Chu et al., 2019).

Based on the tests conducted, it can be concluded that radical and nonradical pathways coexist in the PS-AOP system when using biochar as an activator as depicted in Figure 6. The mechanism changes depending on the biochar prepared from different pyrolysis temperatures. In the case of A350, which is rich in oxygen functional groups including C=O, C–H, and –COOH, these groups can act as electron donors for the production of free radicals. The dominant radical detected is •OH as indicated by the quenching test results. However, the low surface area and less hydrophobic surface limit mass transfer and adsorption, which results in a lower degradation rate constant of BPA. Additionally, although a high Fe content is detected in A350, it is in the form of Fe_3O_4, which is not readily available as an oxidant. A500, with a higher surface area than A350, along with a slightly more hydrophobic surface, promotes both radical and nonradical pathways. As for A700, with a more graphitic and hydrophobic surface, the occurrence of surface-mediated transfer increases. Thus, it is safe to speculate that the nonradical pathway played an important role in the degradation of the BPA of this system. It has also been reported that a high graphitization biochar structure increases mediated electron transfer (Wang et al., 2018; Yu, Tang, Pang, Zeng, Feng, Zou, Wang, Feng, Zhu, Ouyang and Tan, 2020).

3.4 Effect of water chemistry

The pH of the solution plays a critical role in activating PDS. It affects not only the stability and speciation of radicals but also the forms of BPA and the surface charges of SBC (Huang et al., 2021). To investigate the influence of pH on BPA degradation by PS-AOP using

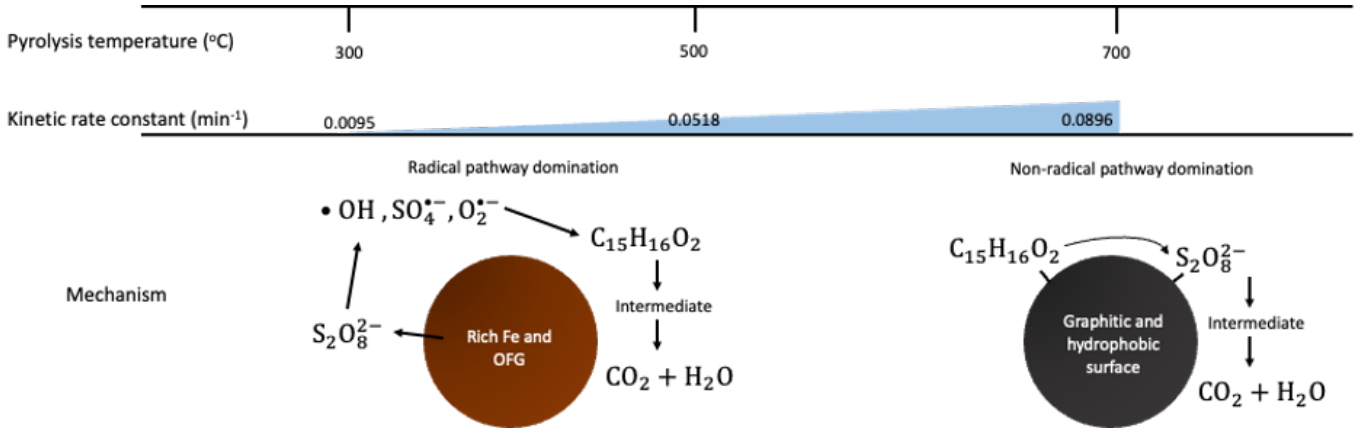

Figure 6 Overall reaction scheme.

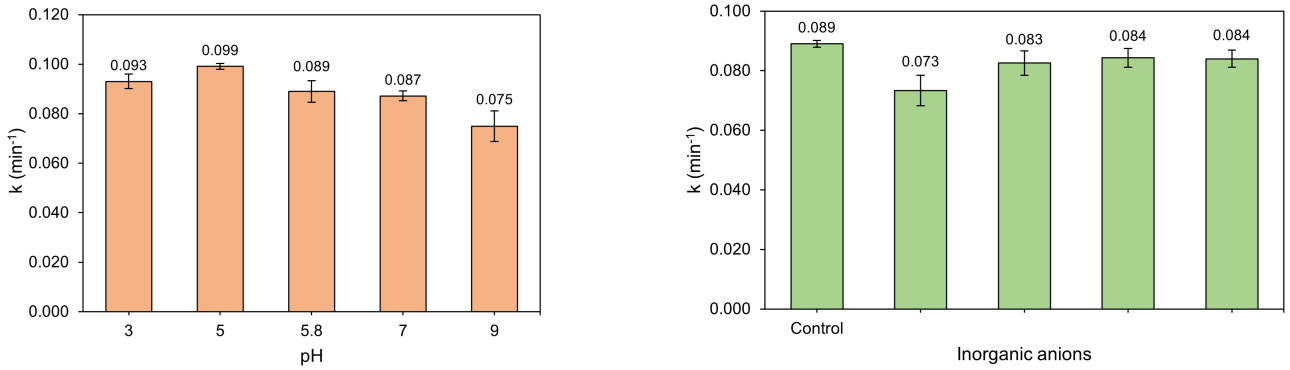

(a) pH (b) Inorganic anions

Figure 7 Effect of (a) pH and (b) inorganic anions on the rate constant of PS-AOP for the A700 system (α = 0.05, pH 9 *p*-value = 0.0469, Cl^- *p*-value = 0.0277).

A700, which exhibits the highest kinetic activity, experiments were conducted at initial pH values of 3, 5, 7, and 9. Additionally, experiments were conducted at an unadjusted initial pH of 5.8. As depicted in Figure 7a, a difference of 11%–18% in rate constants was observed with the unadjusted pH (5.8). Furthermore, a t-test was performed to determine whether significant differences existed between the various pH values and the unadjusted pH. According to the results, only the initial pH of 9 showed a significant difference (Table S5 Appendix A). pH values below 9, which are below the pKa value of BPA, resulted in no significant changes. However, when the initial pH surpasses the pKa value, the deprotonated form of BPA becomes dominant (Fan et al., 2021). This negatively charged phenoxide form of BPA is repelled by the negatively charged biochar surface as the pH is far above the pH_{pzc} (Table 2). Consequently, a decrease in the rate constant is observed at a pH value of 9. This result demonstrates that the performance of the system is not pH-dependent and suggests that the process can operate effectively within a wide pH range, which is advantageous for real-world applications.

Cl^-, NO_3^-, SO_4^{2-}, and HCO_3^- are the major inorganic anions in aquatic environments, and their effects on PS-AOP have been reported to either promote or inhibit the process (Ghanbari and Moradi, 2017). Therefore, it is essential to conduct a thorough analysis of the influences of these ions for the real-world application of wastewater treatment. A slight decrease in the rate constant ranging from 5.5% to 19.6% was observed as shown in Figure 7b. Based on the t-test results, only the presence of Cl^- shows a significant difference in the rate constant relative to conditions without anions (Table S6 Appendix A). The influence of Cl^- in decreasing the rate constant might be due to $O_2^{\bullet-}$ as the dominant active species in the A700 system. The presence of Cl^- has been reported to decrease the generation of $O_2^{\bullet-}$ because Cl^- and $O_2^{\bullet-}$ might react to form oxygen (Ahmad et al., 2015; Koppenol, 1994). However, the presence of NO_3^-, SO_4^{2-}, and HCO_3^- does not significantly alter the rate constant. The concentration of inorganic anions used in the study ranges from 700 to 1000 mgL^{-1}, which is higher than the typical concentration range of common inorganic anions in surface water (Saha et al., 2022). This ensures that the pres-

ence of inorganic anions in real surface water samples will not affect the pollutant removal results. In general, the presence of inorganic anions is less likely to disrupt the oxidation process because of the predominance of nonradical pathways over radical formation (Ren et al., 2022).

4 CONCLUSION

Sludge originating from the aerobic digestion of sewage treatment was converted into biochar at varying pyrolysis temperatures to investigate the effect of this parameter on persulfate activation for BPA degradation. A350, characterized by an abundance of surface functional groups such as C=O and -COOH, contributed to the formation of free radicals. Quenching tests revealed the presence of •OH radicals in this system. Additionally, A350 exhibited the highest Fe content, albeit in an amorphous form and therefore not readily available to serve as active sites for radical production, which resulted in a lower BPA degradation rate constant. With the increase in its surface area, the A500 system demonstrated a higher rate constant than A350. Quenching tests indicated a greater presence of radicals participating in BPA degradation due to the availability of more surface-active sites. A700 showed the highest rate constant value of $8.96 \times 10^{-2} min^{-1}$, characterized by low O/C and I_D/I_G values, which indicate a hydrophobic and graphitized structure. These features led to the dominance of nonradical pathways as indicated by quenching tests, which demonstrated that this system was unaffected by chemical quenching. Furthermore, persulfate consumption increased only in the presence of BPA, PS, and SBC. The A500 and A700 systems were predominantly driven by the oxidation process based on fraction tests. However, continued low adsorption was detected when A350 was used, which suggests that SBC prepared above 500 °C is preferable for catalyst preparation. BPA degradation by PS-AOP using A700 was negligibly affected by water matrix factors, including pH values ranging from 3 to 9 and inorganic anions including Cl^-, NO_3^-, SO_4^{2-}, and HCO_3^-.

The novelty of this study lies in the use of a specific type of sludge from sewage treatment and confirms that different unit processes produce varying sludge properties, which in turn influence the properties of biochar. Traditionally, the use of sewage sludge has been generalized without consideration for its origin or the diverse properties it can impart to biochar. Moreover, this study provides a systematic insight into the effects of pyrolysis temperature on biochar properties, oxidation performance, and pathways. Nevertheless, there are further areas for improvement to address. These include additional ROS detection using Electron Paramagnetic Resonance methods, testing the reusability of biochar, and evaluating its application in actual water bodies. These enhancements would enrich the study and offer a novel, value-added approach to reusing sewage sludge as an efficient persulfate activator that exhibits good resistance to water matrix conditions.

DISCLAIMER

The authors declare no conflict of interest.

ACKNOWLEDGMENTS

This research was supported by AOP System Laboratory; School of Civil, Environmental, and Architectural Engineering; Korea University.

REFERENCES

Ahmad, A., Gu, X., Li, L., Lu, S., Xu, Y. and Guo, X. (2015), 'Effects of ph and anions on the generation of reactive oxygen species (ros) in nzvi-rgo-activated persulfate system', *Water, Air, Soil Pollution* **226**(11), 369.
URL: *https://doi.org/10.1007/s11270-015-2635-8*

Bai, X., Zhang, Y., Shi, J., Xu, L., Wang, Y. and Jin, P. (2021), 'A new application pattern for sludge-derived biochar adsorbent: Ideal persulfate activator for the high-efficiency mineralization of pollutants', *Journal of Hazardous Materials* **419**, 126343.
URL: *https://doi.org/10.1016/j.jhazmat.2021.126343*

Chen, Y., Duan, X., Zhang, C., Wang, S., Ren, N. and Ho, S.-H. (2020), 'Graphitic biochar catalysts from anaerobic digestion sludge for nonradical degradation of micropollutants and disinfection', *Chemical Engineering Journal* **384**, 123244.
URL: *https://doi.org/10.1016/j.cej.2019.123244*

Chen, Y., Wang, R., Duan, X., Wang, S., Ren, N. and Ho, S.-H. (2020), 'Production, properties, and catalytic applications of sludge derived biochar for environmental remediation', *Water Research* **187**, 116390.
URL: *https://doi.org/10.1016/j.watres.2020.116390*

Chen, Z., Jin, J., Song, X., Zhang, G. and Zhang, S. (2018), 'Redox conversion of arsenite and nitrate in the uv/quinone systems', *Environmental Science Technology* **52**(17), 10011–10018.
URL: *https://doi.org/10.1021/acs.est.8b03538*

Cheng, X., Guo, H., Zhang, Y., Wu, X. and Liu, Y. (2017), 'Non-photochemical production of singlet oxygen via activation of persulfate by carbon nanotubes', *Water Research* **113**, 80–88.
URL: *https://doi.org/10.1016/j.watres.2017.02.016*

Chu, C., Yang, J., Huang, D., Li, J., Wang, A., Alvarez, P. J. J. and Kim, J.-H. (2019), 'Cooperative pollutant adsorption and persulfate-driven oxidation on hierarchically ordered porous carbon', *Environmental Science*

Technology **53**(17), 10352–10360.
URL: *https://doi.org/10.1021/acs.est.9b03067*

Corrales, J., Kristofco, L. A., Steele, W. B., Yates, B. S., Breed, C. S., Williams, E. S. and Brooks, B. W. (2015), 'Global assessment of bisphenol a in the environment: Review and analysis of its occurrence and bioaccumulation', *Dose-Response* **13**(3), 1559325815598308.
URL: *https://doi.org/10.1177/1559325815598308*

Diao, Z.-H., Dong, F.-X., Yan, L., Chen, Z.-L., Qian, W., Kong, L.-J., Zhang, Z.-W., Zhang, T., Tao, X.-Q., Du, J.-J., Jiang, D. and Chu, W. (2020), 'Synergistic oxidation of bisphenol a in a heterogeneous ultrasound-enhanced sludge biochar catalyst/persulfate process: Reactivity and mechanism', *Journal of Hazardous Materials* **384**, 121385.
URL: *https://doi.org/10.1016/j.jhazmat.2019.121385*

Fan, X., Lin, H., Zhao, J., Mao, Y., Zhang, J. and Zhang, H. (2021), 'Activation of peroxymonosulfate by sewage sludge biochar-based catalyst for efficient removal of bisphenol a: Performance and mechanism', *Separation and Purification Technology* **272**, 118909.
URL: *https://doi.org/10.1016/j.seppur.2021.118909*

Gao, Y., Chen, Y., Song, T., Su, R. and Luo, J. (2022), 'Activated peroxymonosulfate with ferric chloride-modified biochar to degrade bisphenol a: Characteristics, influencing factors, reaction mechanism and reuse performance', *Separation and Purification Technology* **300**, 121857.
URL: *https://doi.org/10.1016/j.seppur.2022.121857*

Gasim, M. F., Lim, J.-W., Low, S.-C., Lin, K.-Y. A. and Oh, W.-D. (2022), 'Can biochar and hydrochar be used as sustainable catalyst for persulfate activation?', *Chemosphere* **287**, 132458.
URL: *https://doi.org/10.1016/j.chemosphere.2021.132458*

Ghanbari, F. and Moradi, M. (2017), 'Application of peroxymonosulfate and its activation methods for degradation of environmental organic pollutants: Review', *Chemical Engineering Journal* **310**, 41–62.
URL: *https://doi.org/10.1016/j.cej.2016.10.064*

Ghodake, G. S., Shinde, S. K., Kadam, A. A., Saratale, R. G., Saratale, G. D., Kumar, M., Palem, R. R., AL-Shwaiman, H. A., Elgorban, A. M., Syed, A. and Kim, D.-Y. (2021), 'Review on biomass feedstocks, pyrolysis mechanism and physicochemical properties of biochar: State-of-the-art framework to speed up vision of circular bioeconomy', *Journal of Cleaner Production* **297**, 126645.
URL: *https://doi.org/10.1016/j.jclepro.2021.126645*

Ginter-Kramarczyk, D., Zembrzuska, J., Kruszelnicka, I., Zając-Woźnialis, A. and Ciślak, M. (2022), 'Influence of temperature on the quantity of bisphenol a in bottled drinking water', *International Journal of Environmental Research and Public Health* **19**(9), Article 9.
URL: *https://doi.org/10.3390/ijerph19095710*

Gokulakrishnan, S., Mohammed, A. and Prakash, H. (2016), 'Determination of persulphates using n,n-diethyl-p-phenylenediamine as colorimetric reagent: Oxidative coloration and degradation of the reagent without bactericidal effect in water', *Chemical Engineering Journal* **286**, 223–231.
URL: *https://doi.org/10.1016/j.cej.2015.10.058*

Gopinath, A., Divyapriya, G., Srivastava, V., Laiju, A. R., Nidheesh, P. V. and Kumar, M. S. (2021), 'Conversion of sewage sludge into biochar: A potential resource in water and wastewater treatment', *Environmental Research* **194**, 110656.
URL: *https://doi.org/10.1016/j.envres.2020.110656*

Guo, W.-Q., Yang, S.-S., Xiang, W.-S., Wang, X.-J. and Ren, N.-Q. (2013), 'Minimization of excess sludge production by in-situ activated sludge treatment processes—a comprehensive review', *Biotechnology Advances* **31**(8), 1386–1396.
URL: *https://doi.org/10.1016/j.biotechadv.2013.06.003*

Hu, L., Wang, P., Shen, T., Wang, Q., Wang, X., Xu, P., Zheng, Q. and Zhang, G. (2020), 'The application of microwaves in sulfate radical-based advanced oxidation processes for environmental remediation: A review', *Science of The Total Environment* **722**, 137831.
URL: *https://doi.org/10.1016/j.scitotenv.2020.137831*

Hu, W., Tong, W., Li, Y., Xie, Y., Chen, Y., Wen, Z., Feng, S., Wang, X., Li, P., Wang, Y. and Zhang, Y. (2020), 'Hydrothermal route-enabled synthesis of sludge-derived carbon with oxygen functional groups for bisphenol a degradation through activation of peroxymonosulfate', *Journal of Hazardous Materials* **388**, 121801.
URL: *https://doi.org/10.1016/j.jhazmat.2019.121801*

Huang, B.-C., Jiang, J., Huang, G.-X. and Yu, H.-Q. (2018), 'Sludge biochar-based catalysts for improved pollutant degradation by activating peroxymonosulfate', *Journal of Materials Chemistry A* **6**(19), 8978–8985.
URL: *https://doi.org/10.1039/C8TA02282H*

Huang, W., Xiao, S., Zhong, H., Yan, M. and Yang, X. (2021), 'Activation of persulfates by carbonaceous materials: A review', *Chemical Engineering Journal* **418**, 129297.
URL: *https://doi.org/10.1016/j.cej.2021.129297*

Hwang, S., Huling, S. G. and Ko, S. (2010), 'Fenton-like degradation of mtbe: Effects of iron counter anion and radical scavengers', *Chemosphere* **78**(5), 563–568.
URL: *https://doi.org/10.1016/j.chemosphere.2009.11.005*

Janu, R., Mrlik, V., Ribitsch, D., Hofman, J., Sedláček, P., Bielská, L. and Soja, G. (2021), 'Biochar surface functional groups as affected by biomass feedstock, biochar composition and pyrolysis temperature', *Carbon Resources Conversion* **4**, 36–46.
URL: *https://doi.org/10.1016/j.crcon.2021.01.003*

Ji, J., Yuan, X., Zhao, Y., Jiang, L. and Wang, H. (2022), 'Mechanistic insights of removing pollutant in adsorption and advanced oxidation processes by sludge biochar', *Journal of Hazardous Materials* **430**, 128375.
URL: *https://doi.org/10.1016/j.jhazmat.2022.128375*

Jiang, L. et al. (2020), 'Role of adsorption and oxidation in porous carbon aerogel/persulfate system for non-radical degradation of organic contaminant', *Chemosphere* **241**, 125066.
URL: *https://doi.org/10.1016/j.chemosphere.2019.125066*

Kamal, F. M., Laksono, S. and Adityosulindro, S. (2024), 'Advanced treatment: Tackling paracetamol with fenton oxidation and membrane hybrid processes', *Journal of the Civil Engineering Forum* pp. 279–286.
URL: *https://doi.org/10.22146/jcef.13031*

Keiluweit, M., Nico, P. S., Johnson, M. G. and Kleber, M. (2010), 'Dynamic molecular structure of plant biomass-derived black carbon (biochar)', *Environmental Science Technology* **44**(4), 1247–1253.
URL: *https://doi.org/10.1021/es9031419*

Koppenol, W. H. (1994), 'Thermodynamic considerations on the formation of reactive species from hypochlorite, superoxide and nitrogen monoxide: Could nitrosyl chloride be produced by neutrophils and macrophages?', *FEBS Letters* **347**(1), 5–8.
URL: *https://doi.org/10.1016/0014-5793(94)00494-3*

Lee, J., von Gunten, U. and Kim, J.-H. (2020), 'Persulfate-based advanced oxidation: Critical assessment of opportunities and roadblocks', *Environmental Science Technology* **54**(6), 3064–3081.
URL: *https://doi.org/10.1021/acs.est.9b07082*

Leng, L., Xiong, Q., Yang, L., Li, H., Zhou, Y., Zhang, W., Jiang, S., Li, H. and Huang, H. (2021), 'An overview on engineering the surface area and porosity of biochar', *Science of The Total Environment* **763**, 144204.
URL: *https://doi.org/10.1016/j.scitotenv.2020.144204*

Li, F., Duan, F., Ji, W. and Gui, X. (2020), 'Biochar-activated persulfate for organic contaminants removal: Efficiency, mechanisms and influencing factors', *Ecotoxicology and Environmental Safety* **198**, 110653.
URL: *https://doi.org/10.1016/j.ecoenv.2020.110653*

Li, J., Wan, Y., Li, Y., Yao, G. and Lai, B. (2019), 'Surface fe(iii)/fe(ii) cycle promoted the degradation of atrazine by peroxymonosulfate activation in the presence of hydroxylamine', *Applied Catalysis B: Environmental* **256**, 117782.
URL: *https://doi.org/10.1016/j.apcatb.2019.117782*

Liang, C., Huang, C.-F., Mohanty, N. and Kurakalva, R. M. (2008), 'A rapid spectrophotometric determination of persulfate anion in isco', *Chemosphere* **73**(9), 1540–1543.
URL: *https://doi.org/10.1016/j.chemosphere.2008.08.043*

Luo, Y., Guo, W., Ngo, H. H., Nghiem, L. D., Hai, F. I., Zhang, J., Liang, S. and Wang, X. C. (2014), 'A review on the occurrence of micropollutants in the aquatic environment and their fate and removal during wastewater treatment', *Science of The Total Environment* **473–474**, 619–641.
URL: *https://doi.org/10.1016/j.scitotenv.2013.12.065*

Marleni, N. N. N., Ermawati, R. and Istiqomah, N. A. (2021), 'The application of combined phytoremediation greywater treatment in a single house', *Journal of the Civil Engineering Forum* **7**(1), 47–58.
URL: *https://doi.org/10.22146/jcef.58218*

Mian, M. M., Liu, G. and Fu, B. (2019), 'Conversion of sewage sludge into environmental catalyst and microbial fuel cell electrode material: A review', *Science of The Total Environment* **666**, 525–539.
URL: *https://doi.org/10.1016/j.scitotenv.2019.02.200*

Mpatani, F. M., Han, R., Aryee, A. A., Kani, A. N., Li, Z. and Qu, L. (2021), 'Adsorption performance of modified agricultural waste materials for removal of emerging micro-contaminant bisphenol a: A comprehensive review', *Science of The Total Environment* **780**, 146629.
URL: *https://doi.org/10.1016/j.scitotenv.2021.146629*

Oh, W.-D., Dong, Z., Ronn, G. and Lim, T.-T. (2017), 'Surface-active bismuth ferrite as superior peroxymonosulfate activator for aqueous sulfamethoxazole removal: Performance, mechanism and quantification of sulfate radical', *Journal of Hazardous Materials* **325**, 71–81.
URL: *https://doi.org/10.1016/j.jhazmat.2016.11.056*

Olmez-Hanci, T. et al. (2018), 'Oxidative degradation of bisphenol a by carbocatalytic activation of persulfate and peroxymonosulfate with reduced graphene oxide', *Journal of Hazardous Materials* **360**, 141–149.
URL: *https://doi.org/10.1016/j.jhazmat.2018.07.098*

Pariyar, P., Kumari, K., Jain, M. K. and Jadhao, P. S. (2020), 'Evaluation of change in biochar properties derived from different feedstock and pyrolysis temperature for environmental and agricultural application', *Science of The Total Environment* **713**, 136433.
URL: *https://doi.org/10.1016/j.scitotenv.2019.136433*

Pei, X.-Y., Ren, H.-Y., Xing, D.-F., Xie, G.-J., Cao, G.-L., Meng, J., Ren, N.-Q. and Liu, B.-F. (2021), 'Electron transfer mechanism of peroxydisulfate activation by sewage sludge-derived biochar for enhanced degradation of sulfamethoxazole', *Environmental Science: Water Research Technology* **7**(9), 1563–1575.
URL: *https://doi.org/10.1039/D1EW00279A*

Ren, W., Cheng, C., Shao, P., Luo, X., Zhang, H., Wang, S. and Duan, X. (2022), 'Origins of electron-transfer regime in persulfate-based nonradical oxidation processes', *Environmental Science Technology* **56**(1), 78–97.
URL: *https://doi.org/10.1021/acs.est.1c05374*

Ren, W. et al. (2019), 'Activation of peroxydisulfate on carbon nanotubes: Electron-transfer mechanism', *Environmental Science & Technology* **53**(24), 14595–14603.
URL: *https://doi.org/10.1021/acs.est.9b05475*

Ronsse, F., van Hecke, S., Dickinson, D. and Prins, W. (2013), 'Production and characterization of slow pyrolysis biochar: Influence of feedstock type and pyrolysis conditions', *GCB Bioenergy* **5**(2), 104–115.
URL: *https://doi.org/10.1111/gcbb.12018*

Saha, A., Ahweyevu, J. O., Baker, E. M., Penn, D. and Saha, S. (2022), 'Assessment of common anion and cation contaminants in surface waterbodies in statesboro, georgia, usa', *Earth Systems and Environment* **6**(2), 617–630.
URL: *https://doi.org/10.1007/s41748-022-00300-6*

Shaheen, J., Fseha, Y. H. and Sizirici, B. (2022), 'Performance, life cycle assessment, and economic comparison between date palm waste biochar and activated carbon derived from woody biomass', *Heliyon* **8**(12).
URL: *https://doi.org/10.1016/j.heliyon.2022.e12388*

Shao, L., Wang, T., Li, T., Lü, F. and He, P. (2013), 'Comparison of sludge digestion under aerobic and anaerobic conditions with a focus on the degradation of proteins at mesophilic temperature', *Bioresource Technology* **140**, 131–137.
URL: *https://doi.org/10.1016/j.biortech.2013.04.081*

Shao, Y., Tian, C., Yang, Y., Shao, Y., Zhang, T., Shi, X., Zhang, W. and Zhu, Y. (2022), 'Carbothermal synthesis of sludge biochar supported nanoscale zero-valent iron for the removal of cd2+ and cu2+: Preparation, performance, and safety risks', *International Journal of Environmental Research and Public Health* **19**(23), 16041.
URL: *https://doi.org/10.3390/ijerph192316041*

Song, G., Qin, F., Yu, J., Tang, L., Pang, Y., Zhang, C., Wang, J. and Deng, L. (2022), 'Tailoring biochar for persulfate-based environmental catalysis: Impact of biomass feedstocks', *Journal of Hazardous Materials* **424**, 127663.
URL: *https://doi.org/10.1016/j.jhazmat.2021.127663*

Tratnyek, P., Powell, J. and Waldemer, R. (2009), Improved understanding of in situ chemical oxidation. technical objective i: Contaminant oxidation kinetics, Technical report, U.S. Department of Defense. Contaminant Oxidation Kinetics Report, 59 pp.

Wang, J., Liao, Z., Ifthikar, J., Shi, L., Du, Y., Zhu, J., Xi, S., Chen, Z. and Chen, Z. (2017), 'Treatment of refractory contaminants by sludge-derived biochar/persulfate system via both adsorption and advanced oxidation process', *Chemosphere* **185**, 754–763.
URL: *https://doi.org/10.1016/j.chemosphere.2017.07.084*

Wang, J., Wang, C., Guo, H., Ye, T., Liu, Y., Cheng, X., Li, W., Yang, B. and Du, E. (2020), 'Crucial roles of oxygen and superoxide radical in bisulfite-activated persulfate oxidation of bisphenol af: Mechanisms, kinetics and dft studies', *Journal of Hazardous Materials* **391**, 122228.
URL: *https://doi.org/10.1016/j.jhazmat.2020.122228*

Wang, N., Ma, W., Ren, Z., Du, Y., Xu, P. and Han, X. (2018), 'Prussian blue analogues derived porous nitrogen-doped carbon microspheres as high-performance metal-free peroxymonosulfate activators for non-radical-dominated degradation of organic pollutants', *Journal of Materials Chemistry A* **6**(3), 884–895.
URL: *https://doi.org/10.1039/C7TA08472B*

Wang, X., Gu, L., Zhou, P., Zhu, N., Li, C., Tao, H., Wen, H. and Zhang, D. (2017), 'Pyrolytic temperature dependent conversion of sewage sludge to carbon catalyst and their performance in persulfate degradation of 2-naphthol', *Chemical Engineering Journal* **324**, 203–215.
URL: *https://doi.org/10.1016/j.cej.2017.04.101*

Wang, Z.-J., Lin, Y.-Q., Zhou, H.-J., Liu, Z.-L., Miao, R.-R., Xu, X.-M., He, L. and Guan, Q.-Q. (2023), 'Boosting persulfate activation via paper mill sludge-based biochar for efficient degradation of bisphenol a: Inherent multiple active sites', *Chemical Engineering Journal* **455**, 140795.
URL: *https://doi.org/10.1016/j.cej.2022.140795*

Wilkinson, F., Helman, W. P. and Ross, A. B. (1995*a*), 'Rate constants for the decay and reactions of the lowest electronically excited singlet state of molecular oxygen in solution. an expanded and revised compilation', *Journal of Physical and Chemical Reference Data* **24**(2), 663–677.
URL: *https://doi.org/10.1063/1.555965*

Wilkinson, F., Helman, W. P. and Ross, A. B. (1995*b*), 'Rate constants for the decay and reactions of the lowest electronically excited singlet state of molecular oxygen in solution. an expanded and revised compilation', *Journal of Physical and Chemical Reference Data* **24**(2), 663–677.
URL: *https://doi.org/10.1063/1.555965*

Wu, W., Zhu, S., Huang, X., Wei, W. and Ni, B.-J. (2021), 'Mechanisms of persulfate activation on biochar derived from two different sludges: Dominance of their intrinsic compositions', *Journal of Hazardous Materials* **408**, 124454.
URL: *https://doi.org/10.1016/j.jhazmat.2020.124454*

Xiao, P., Yi, X., Wu, M., Wang, X., Zhu, S., Gao, B., Liu, Y. and Zhou, H. (2022), 'Catalytic performance and periodate activation mechanism of anaerobic sewage sludge-derived biochar', *Journal of Hazardous Materials* **424**, 127692.
URL: *https://doi.org/10.1016/j.jhazmat.2021.127692*

Yu, J., Feng, H., Tang, L., Pang, Y., Zeng, G., Lu, Y., Dong, H., Wang, J., Liu, Y., Feng, C., Wang, J., Peng, B. and Ye, S. (2020), 'Metal-free carbon materials for persulfate-based advanced oxidation process: Microstructure, property and tailoring', *Progress in Materials Science* **111**, 100654.
URL: *https://doi.org/10.1016/j.pmatsci.2020.100654*

Yu, J., Tang, L., Pang, Y., Zeng, G., Feng, H., Zou, J., Wang, J., Feng, C., Zhu, X., Ouyang, X. and Tan, J. (2020), 'Hierarchical porous biochar from shrimp shell for persulfate activation: A two-electron transfer path and key impact factors', *Applied Catalysis B: Environmental* **260**, 118160.
URL: *https://doi.org/10.1016/j.apcatb.2019.118160*

Zhang, Y., Dai, M. and Yuan, Z. (2018), 'Methods for the detection of reactive oxygen species', *Analytical Methods* **10**(38), 4625–4638.
URL: *https://doi.org/10.1039/C8AY01339J*

Zhao, Y., Song, M., Cao, Q., Sun, P., Chen, Y. and Meng, F. (2020), 'The superoxide radicals' production via persulfate activated with cufe2o4@biochar composites to promote the redox pairs cycling for efficient degradation of o-nitrochlorobenzene in soil', *Journal of Hazardous Materials* **400**, 122887.
URL: *https://doi.org/10.1016/j.jhazmat.2020.122887*

Zhou, C., Gao, N., Li, R. and Deng, Y. (2015), 'Desorption of bisphenol-a (bpa) and regeneration of bpa-spent granular activated carbon using ultrasonic irradiation and organic solvent extraction', *Desalination and Water Treatment* **54**(11), 3106–3113.
URL: *https://doi.org/10.1080/19443994.2014.912961*

Zhou, T., Shi, C., Wang, Y., Wang, X., Lei, Z., Liu, X., Wu, J., Luo, F. and Wang, L. (2024), 'Progress of metal-loaded biochar-activated persulfate for degradation of emerging organic contaminants', *Water Science and Technology* **90**(3), 824–843.
URL: *https://doi.org/10.2166/wst.2024.256*

Zhou, X., Lai, C., Almatrafi, E., Liu, S., Yan, H., Qian, S., Li, H., Qin, L., Yi, H., Fu, Y., Li, L., Zhang, M., Xu, F., Zeng, Z. and Zeng, G. (2023), 'Unveiling the roles of dissolved organic matters derived from different biochar in biochar/persulfate system: Mechanism and toxicity', *Science of The Total Environment* **864**, 161062.
URL: *https://doi.org/10.1016/j.scitotenv.2022.161062*

Zhou, X., Wei, J., Liu, K., Liu, N. and Zhou, B. (2014), 'Adsorption of bisphenol a based on synergy between hydrogen bonding and hydrophobic interaction', *Langmuir* **30**(46), 13861–13868.
URL: *https://doi.org/10.1021/la502816m*

Zhou, X., Zhu, Y., Niu, Q., Zeng, G., Lai, C., Liu, S., Huang, D., Qin, L., Liu, X., Li, B., Yi, H., Fu, Y., Li, L., Zhang, M., Zhou, C. and Liu, J. (2021), 'New notion of biochar: A review on the mechanism of biochar applications in advanced oxidation processes', *Chemical Engineering Journal* **416**, 129027.
URL: *https://doi.org/10.1016/j.cej.2021.129027*

Zielińska, A., Oleszczuk, P., Charmas, B., Skubiszewska-Zięba, J. and Pasieczna-Patkowska, S. (2015), 'Effect of sewage sludge properties on the biochar characteristic', *Journal of Analytical and Applied Pyrolysis* **112**, 201–213.
URL: *https://doi.org/10.1016/j.jaap.2015.01.025*

APPENDIX A

Text S1 Adsorption kinetics

The equation for pseudo-first order is given below (Jiang et al., 2020):

$$\frac{q_e - q_t}{q_e} = -k_1 t \tag{4}$$

Pseudo second order kinetic model is represented by:

$$\frac{t}{q_t} = \frac{1}{k_2 q_e^2} + \frac{1}{q_e} t \tag{5}$$

The initial sorption rate is defined by the following equation:

$$h = k_2 q_e^2 \tag{6}$$

k_1 is the pseudo-first order kinetic constant (min^{-1}), q_e and q_t are the amounts of Bisphenol-A adsorbed on the biochar at equilibrium and at time t (min), respectively. Where k_2 is the pseudo-second order rate constant (g $mg^{-1}min^{-1}$) and h is the initial adsorption rate (g $mg^{-1}min^{-1}$).

Table S1. Sludge physicochemical properties

Sample	Proximate analysis			Ultimate analysis															
	Organic element		Inorganic element	Organic element (wt%)							Inorganic element (wt%)								
	Protein (μg/mL)	Polysaccharide (μg/mL)	Ash (wt%)	C	H	N	S	O	O/C	H/C	Mn	Fe	Cu	Zn	Si	P	K	Ca	Ti
Sludge	95.47	15.28	63.6	25.8	2.1	5.69	0.27	30	1.16	0.08	2.50	36.01	1.06	2.01	15.85	18.56	6.68	15.57	1.72

Table S2. Parameters of the pseudo first-order and second-order kinetic models for BPA adsorption on sludge biochar

Biochar	Pseudo first-order			Second order			
	q_e (mg g^{-1})	K_1 (10^{-4} mg $g^{-1}min^{-1}$)	r^2	q_e (mg g^{-1})	K_2 (10^{-4} mg g^{-1} min^{-1})	h	r^2
A350	6.26	98	0.75	11.62	15	0.20	0.91
A500	5.55	111	0.64	14.22	16	0.13	0.90
A700	6.27	152	0.54	12.16	22	0.33	0.92

Table S3. Comparison of catalytic performances of A700 with similar catalytic systems using carbonaceous materials for BPA degradation.

Catalyst	Synthesis parameters	Surface area (m^2g^{-1})	Experiment condition	Rate constant (min^{-1})	Ref.
rGO	Commercial	287.52	$[BPA]_0$= 2 mg/L; $[catalyst]_0$= 0.02 g/L; $[PDS]_0$= 0.50 mM; pH= 6.5; T= 25 °C	7.3	Olmez-Hanci et al. (2018)
CNT	Commercial	⩾700	$[BPA]_0$= 20 mg/L; $[catalyst]_0$= 0.1 g/L; $[PDS]_0$= 1.0 mM; pH= 7.3; T= 25 °C	4	Ren et al. (2019)
Paper mill sludge biochar	950 °C, 1.5 h, 5 °C min^{-1}, N_2, no modification	163.35	$[BPA]_0$= 20 mg/L; $[catalyst]_0$= 0.4 g/L; $[PDS]_0$= 5.0 mM; pH= without pH; T= 25 °C	8.5	Wang et al. (2023)
Rice husks biochar	800 °C, 2 h, 10 °C min^{-1}, N_2, ferric chloride-modified	264.5	$[BPA]_0$= 20 mg/L; $[catalyst]_0$= 1.0 g/L; $[PDS]_0$= 6.0 mM; pH= 6.0; T= 25 °C	2.9	Gao et al. (2022)
Sewage sludge biochar	500 °C, 2h, 5 °C min^{-1}, N_2, no modification	115.7	$[BPA]_0$= 10 mg/L; $[catalyst]_0$= 0.07 g/L; $[PDS]_0$= 0.5 mM; pH= 6.0;	0.14	Bai et al. (2021)
Sewage sludge biochar	600 °C, 6h, 5 °C min^{-1}, NH_3, HCl washing	180	$[BPA]_0$= 10 mg/L; $[catalyst]_0$= 0.2 g/L; $[PDS]_0$= 0.16 mM; pH= 6.0;	2	Huang et al. (2018)
Sewage sludge biochar	700 °C, 2 h, 5 °C min^{-1}, N_2, no modification	46	$[BPA]_0$= 50 mg/L; $[catalyst]_0$= 1 g/L; $[PDS]_0$= 1 mM; pH= 5.8; T= 25 °C	8.9	This work

Table S4. *t*-test result for PDS consumption rate data with and without the presence of BPA (*p*-value=0.05)

k data	in DIW	in BPA	*p*-value	difference
A350	0.0063	0.0090	0.0102	significant
A500	0.0080	0.0099		
A700	0.0093	0.0110		

Table S5. *t*-test result for rate constant data pH effect observation (*p*-value=0.05)

pH	pH 3	pH 5	pH 5.8	pH 7	pH 9
k1	0.0934	0.0997	0.0896	0.0872	0.0728
k2	0.0958	0.0998	0.0901	0.0891	0.0819
k3	0.0899	0.0978	0.0823	0.0852	0.0701
p-value	0.1347	0.0506	-	0.9547	0.0469
difference	not significant	not significant	-	not significant	significant

Table S6. *t*-test result for rate constant data inorganic anions effect observation (*p*-value=0.05)

ion	control	Cl^-	NO_3^-	$S0_4^{2-}$	HCO_3^-
k1	0.0896	0.072	0.0805	0.0846	0.0828
k2	0.0904	0.079	0.0873	0.0874	0.0873
k3	0.0882	0.069	0.0799	0.0811	0.0819
p-value	-	0.0277	0.0935	0.0969	0.0689
difference	-	significant	not significant	not significant	not significant

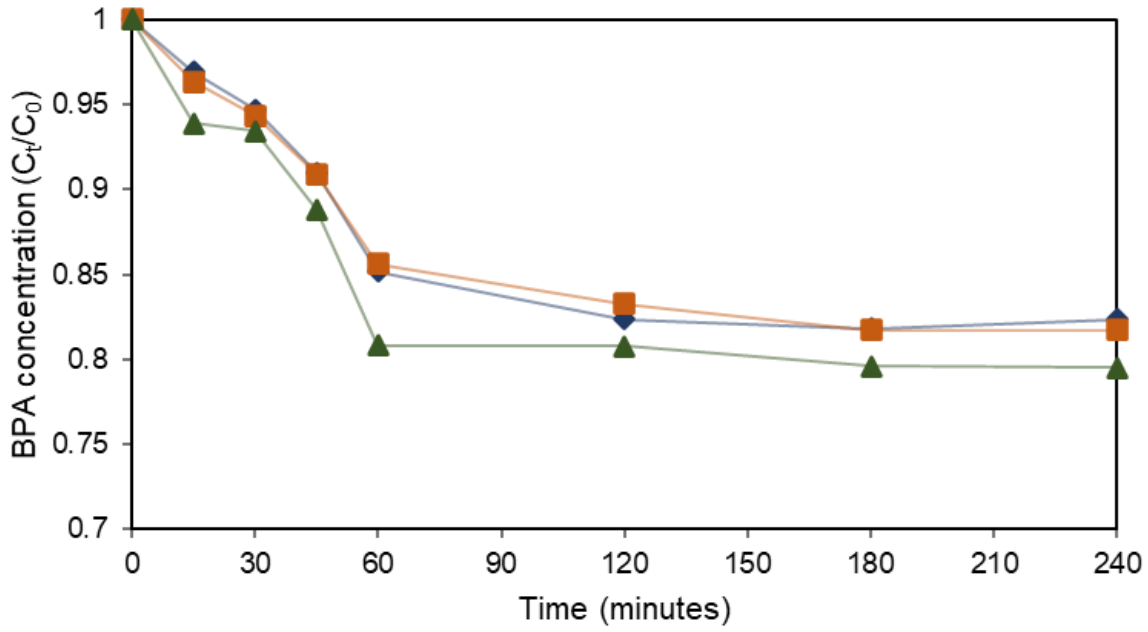

Figure S1 Adsorption of BPA onto SBC. Experimental conditions: Biochar = 1 g L^{-1}; $[BPA]_0$ = 50 mg L^{-1}; T = 298 K, and no pH adjustment.